remote sensing

MDPI

Article

Revealing Water Storage Changes and Ecological Water Conveyance Benefits in the Tarim River Basin over the Past 20 Years Based on GRACE/GRACE-FO

Weicheng Sun and Xingfu Zhang *

School of Civil Transportation Engineering, Guangdong University of Technology, Guangzhou 510006, China; 2112209047@mail2.gdut.edu.cn

* Correspondence: xfzhang77@gdut.edu.cn

Abstract: As China's largest inland river basin and one of the world's most arid regions, the Tarim River Basin is home to an extremely fragile ecological environment. Therefore, monitoring the water storage changes is critical for enhancing water resources management and improving hydrological policies to ensure sustainable development. This study reveals the spatiotemporal changes of water storage and its driving factors in the Tarim River Basin from 2002 to 2022, utilizing data from GRACE, GRACE-FO (GFO), GLDAS, the glacier model, and measured hydrological data. In addition, we validate GRACE/GFO data as a novel resource that can monitor the ecological water conveyance (EWC) benefits effectively in the lower reaches of the basin. The results reveal that (1) the northern Tarim River Basin has experienced a significant decline in terrestrial water storage (TWS), with an overall deficit that appears to have accelerated in recent years. From April 2002 to December 2009, the groundwater storage (GWS) anomaly accounted for 87.5% of the TWS anomaly, while from January 2010 to January 2020, the ice water storage (IWS) anomaly contributed 57.1% to the TWS anomaly. (2) The TWS changes in the Tarim River Basin are primarily attributed to the changes of GWS and IWS, and they have the highest correlation with precipitation and evapotranspiration, with grey relation analysis (GRA) coefficients of 0.74 and 0.68, respectively, while the human factors mainly affect GWS, with an average GRA coefficient of 0.64. (3) In assessing ecological water conveyance (EWC) benefits, the GRACE/GFO-derived TWS anomaly in the lower reaches of the Tarim River exhibits a good correspondence with the changes of EWC, NDVI, and groundwater levels.

Keywords: GRACE/GRACE-FO; Tarim River Basin; terrestrial water storage; groundwater storage; ecological water conveyance

Citation: Sun, W.; Zhang, X. Revealing Water Storage Changes and Ecological Water Conveyance Benefits in the Tarim River Basin over the Past 20 Years Based on GRACE/GRACE-FO. *Remote Sens.* **2024**, *16*, 4355. https://doi.org/10.3390/rs16234355

Academic Editor: Liming He

Received: 10 October 2024
Revised: 17 November 2024
Accepted: 18 November 2024
Published: 22 November 2024

1. Introduction

Monitoring terrestrial water storage (TWS) changes is crucial for revealing the mechanisms of the global water cycle [1,2], exploring the causes of water storage fluctuations [3,4], and preventing droughts and floods [5,6]. Especially in arid regions, irrational human water usage can lead to prolonged and accelerated artificial droughts [7], severely disrupting ecosystems and water balance systems with irreversible effects [8,9]. The Tarim River Basin is a typical arid region in China where extensive agricultural development since the 1950s has resulted in excessive exploitation of groundwater and depletion of water resources [10]. This activity has led to a reduction in the flow of the Tarim River and the occurrence of prolonged dry periods in the mainstreams and tributaries of downstream rivers [11]. Therefore, the Chinese government implemented an ecological water conveyance (EWC) policy [12], which has cumulatively conveyed about 9.5 billion m^3 of ecological water to the lower reaches of the Tarim River by 2022. Furthermore, global warming has led to the continued retreat of Asian glaciers. Calculations based on ICESat-1,2 show that the continuous mass change of Asian glaciers from 2003 to 2019 was -28 ± 6 Gt/a [13]. Observations from CryoSat-2 also reveal that the elevation in Asian glaciers has been on a downward

trend from 2010 to 2019 [14]. Specifically, the glacier area in the Aksu Prefecture retreated by 309.40 km^2 from 1990 to 2022, with the glacier retreat rate increasing [15]. Given the limited water resources in the Tarim River Basin, improper management of these critical resources will severely hinder regional economic development. Therefore, monitoring TWS changes is crucial for strengthening water resource management and achieving sustainable development in the basin.

Due to the scarcity of meteorological stations and groundwater monitoring wells, the application of traditional technology for monitoring the water storage changes presents significant challenges in the Tarim River Basin. However, GRACE and GFO have become a viable and essential tool for monitoring the changes of TWS, glacier mass, and sea level [16–18]. Previous research has demonstrated that GRACE-derived TWS is highly correlated with annual rainfall in the Tarim River Basin [19]. Additionally, GRACE can monitor groundwater storage (GWS) changes based on the relationship between TWS and GWS [20]. Water balance equations [19,21], principal component analysis [22], downscaling analysis [20,23], and other methods [24,25] have been incorporated into the hydrological study of the Tarim River Basin. Several results indicate that the water storage in the Tarim River Basin generally declines in the long term. It is found that the water storage changes in the Tarim River Basin are primarily dependent on precipitation [26,27]. In addition, it is mainly influenced by evapotranspiration in the southern Tianshan Mountains [20]. The increase in agricultural land area and population has led to the over-exploitation of groundwater, and human factors account for over 50% of GWS change [28]. Notably, the frequency and severity of climate extremes have increased significantly in recent years, leading to more hydroclimatic events [29–31].

Thus, we integrate data from GRACE/GFO, glacier models, and hydrological models to comprehensively investigate the water storage changes and driving factors in the Tarim River Basin over the past 20 years. The main components and driving factors of water storage changes are further identified by independent component and grey relation analyses. Furthermore, EWC constitutes a critical strategy for mitigating drought conditions within the lower reaches of the Tarim River. Current studies evaluate the EWC impacts mainly based on the measured material, remote sensing data, and normalized difference vegetation index (NDVI) [32–34], but these methods do not directly reflect the overall water storage changes. While GRACE/GFO has the capability to directly monitor water storage changes, this study examines the feasibility of GRACE/GFO in detecting the EWC impacts in the lower reaches of Tarim River.

2. Study Area and Datasets

2.1. Study Area

The Tarim River Basin, characterized by extreme terrains such as glaciers and deserts, is located northwest of China, surrounded by the Tianshan Mountains, Kunlun Mountains, and Altun Mountains (see Figure 1). The primary sources of replenishment are glacier meltwater and atmospheric precipitation [35]. The Tarim River Basin belongs to the continental warm temperate extreme arid climate, where rainfall is scarce and evaporation is intense [36]. Moreover, the expansion of farmland and population growth have exacerbated land desertification and river drying, resulting in the lower reaches of the Tarim River being affected by the most severe ecological degradation of the basin [37]. Hence, the EWC project has been carried out to alleviate the drought conditions in the lower reaches of the Tarim River since 2000 [38].

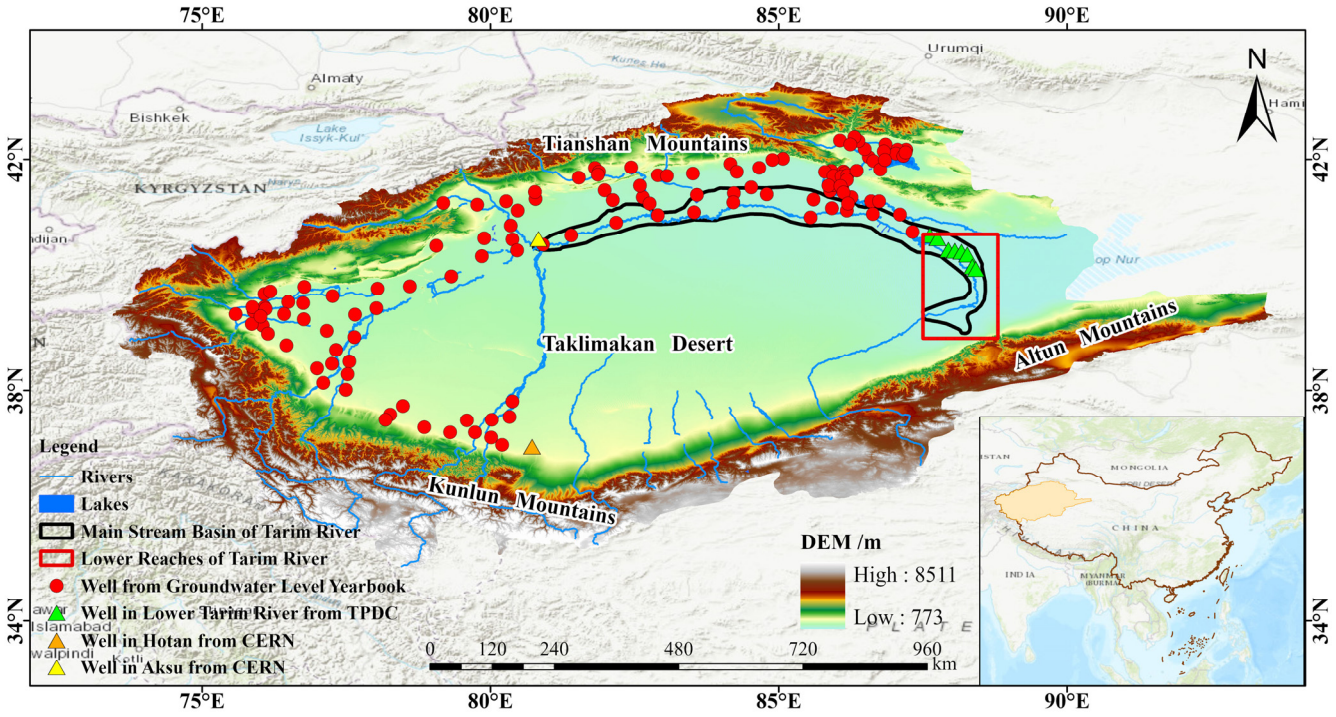

Figure 1. Study area and distribution of groundwater monitoring wells.

2.2. Datasets

The information, sources, and periods of the data models and datasets utilized in this paper can be found in Table 1.

Table 1. Data models and datasets.

Category	Data Information and Source	Period
TWS	CSR GRACE/GFO RL06.2 Mascon (https://www.csr.utexas.edu/, accessed on 27 November 2023) [39]	April 2002–December 2022
SWS	GLDAS NOAH2.1 (https://hydro1.gesdisc.eosdis.nasa.gov/data/, accessed on 25 November 2023)	April 2002–December 2022
IWS	LEGOS Research Team (https://www.sedoo.fr/theia-publication-products/, accessed on 10 November 2023) [40]	April 2002–January 2020
Precipitation	ERA5—Total Precipitation (https://cds.climate.copernicus.eu/, accessed on 18 February 2024)	April 2002–December 2022
Evapotranspiration	ERA5—Evaporation (https://cds.climate.copernicus.eu/, accessed on 18 February 2024)	April 2002–December 2022
Measured GWS	Dataset of Groundwater Level in the lower reaches of Tarim River (https://data.tpdc.ac.cn/, accessed on 5 March 2024) [41]	April 2002–December 2007
	CERN Groundwater Data Set (https://www.scidb.cn/, accessed on 3 March 2024) [42]	January 2005–December 2014
	China Groundwater Level Yearbook for Geo-Environmental Monitoring	January 2018–December 2021
NDVI	MOD13C2 (https://ladsweb.modaps.eosdis.nasa.gov/, accessed on 2 September 2023)	April 2002–December 2022
Runoff	China River Sediment Bulletin	2003–2022
Water consumption	Xinjiang Water Resources Bulletin	2003–2021
EWC	Tarim Basin River Basin Authority	2003–2022

2.2.1. Water Storage Models

The terrestrial water storage anomaly (*TWSA*) is calculated by the Mascon RL06.2 model from the Center for Space Research (CSR) at the University of Texas in Austin,

with a spatial resolution of 0.25° × 0.25°, which is constructed via Tikhonov and L-ribbon regularization. The main improvements compared to the Mascon RL06 model are as follows [39]: (1) the adoption of the new version ACH1B product for GFO accelerometer processing and (2) optimized estimation of the low-order coefficient and elimination of some uncertainty signals. Due to the gaps between GRACE and GFO during the observation process, this study used the Singular Spectrum Analysis (SSA) method to fill the data gaps [43].

For the calculation of surface water storage (SWS), this study used the NOAH v2.1 monthly land surface model from the Global Land Data Assimilation System (GLDAS NOAH v2.1). This model provides global soil moisture storage (SMS), snow water equivalent (SWE), and canopy water storage (CWS), with a spatial resolution of 0.25° × 0.25° and monthly temporal resolution. Additionally, glacier meltwater is also one of the essential sources of replenishment for the Tarim River Basin. This study utilized a glacier model calculated based on DEM and ICESat, which provides global ice water storage (IWS) [40]. After post-processing, a monthly glacier model with a spatial resolution of 0.25° by 0.25° was successfully generated.

2.2.2. Measured Groundwater Data

The measured groundwater data collected in this study are from the National Tibetan Plateau Data Center [41], the Science Data Bank [42], and the China Institute for Geo-Environmental Monitoring. There are 169 groundwater monitoring wells in the Tarim River Basin, and their approximate locations are shown in Figure 1. The measured groundwater data can be converted to a measured GWS anomaly (*GWSA-M*) according to the following equation [44]:

$$GWSA - M = \frac{\sum_{i=1}^{N} S_i \cos(\theta_i) \Delta h_i}{\sum_{i=1}^{N} \cos(\theta_i)} \quad (1)$$

where N represents the number of grids in the study area, S represents the specific yield for the unconfined aquifers or storativity for confined aquifers, θ represents the latitude of each grid, and Δh refers to the mean of groundwater level changes in each grid.

2.2.3. Natural and Human Factors Datasets

The meteorological data are derived from the ERA5 reanalysis dataset, which is obtained by reanalyzing the fifth-generation ECMWF data with global climate observations, providing the best estimate of the atmospheric state. In this study, the monthly scale data of total precipitation and actual evapotranspiration are selected from the ERA5 dataset, where the total precipitation data include rainfall and snowfall, and the total evapotranspiration is the cumulative amount of surface evaporation (including vegetation transpiration), both with a spatial resolution of 0.25° × 0.25°.

The MOD13C2 model, a collaborative effort between the United States Geological Survey (USGS) and the National Aeronautics and Space Administration (NASA), provides monthly high-resolution NDVI data. Furthermore, the Xinjiang Water Resource Bulletin documents the annual water consumption in the Tarim River Basin.

3. Methodology

3.1. Estimation of GWS Change

The TWS is mainly constituted by GWS and SWS. Furthermore, SWS anomaly (*SWSA*) encompasses the anomalies of SMS, SWE, and CWS, thereby facilitating the computation of GWS anomaly (*GWSA*). In addition, this paper separates IWS anomaly (*IWSA*) to derive new *GWSA* (*GWSA-SI*) [45],

$$SWSA = SMSA + SWEA + CWSA \quad (2)$$

$$GWSA = TWSA - SWSA \quad (3)$$

$$GWSA - SI = TWSA - SWSA - IWSA \quad (4)$$

Meanwhile, the instantaneous water storage changes can be obtained from water storage anomalies, taking the instantaneous TWS change (*TWSC*) as an example:

$$TWSC_j = \frac{TWSA_{j+1} - TWSA_{j-1}}{2} \quad (5)$$

where j denotes the month. The remaining instantaneous GWS change (*GWSC*) and instantaneous IWS change (*IWSC*) can be obtained from Equation (5).

3.2. Independent Component Analysis (ICA)

The *TWSA* is comprehensively affected by various periodic signals and long-term trends, which theoretically belong to a mixed signal composed of several independent signal sources. The ICA is an effective signal processing technique for blind source separation, which can separate the mixed signal into multiple independent signal sources based on the maximization of high-order statistics [46].

Based on the information of *TWSA* in GRACE/GFO, a data matrix X of size $m \times n$ can be constructed, where m is the total number of months and n is the number of grids. Through principal component analysis (PCA), we obtain the orthogonal matrix P and the orthogonal eigenvectors E,

$$X_{m\times n} = P_{n\times m} E^T_{n\times m} \quad (6)$$

To separate the mutually independent components as much as possible, an orthogonal rotation matrix is introduced to rotate the principal component (PC) matrix to obtain the ICA decomposition results:

$$X_{m\times n} = P_{n\times r} W_{r\times r} W^T_{r\times r} E^T_{n\times m} = S_{m\times r} A^T_{r\times n} \quad (7)$$

where S and A represent the independent temporal components and spatial patterns, respectively [47], and r is the number of time series or spatial features ($r < n$).

3.3. Drought Index from GRACE/GFO

GRACE-DSI is a drought index from GRACE/GFO-derived TWS, as follows:

$$\text{GRACE} - \text{DSI}_{i,j} = \frac{TWSA_{i,j} - \overline{TWSA_j}}{\sigma_j} \quad (8)$$

where i and j represent the year and month, respectively, $\overline{TWSA_j}$ and σ_j represent the mean and standard deviation of the detrended *TWSA* in month j, respectively. The drought index is divided into six drought categories (see Table 2) [48].

Table 2. Grading criteria for drought.

Drought Category	GRACE-DSI Value
Exceptional drought	≤ -2.00
Extreme drought	-1.99 to -1.60
Severe drought	-1.59 to -1.30
Moderate drought	-1.29 to -0.80
Abnormally dry	-0.79 to -0.50
Normal or wet	≥ -0.49

4. Results

4.1. Spatial and Temporal Changes of Water Storage and NDVI

Figure 2 illustrates the spatial changes of *TWSA*, *IWSA*, *SWSA*, and NDVI in the Tarim River Basin. Specifically, Figure 2a depicts a notable reduction in *TWSA* in the northern part of the basin. This reduction is primarily due to the diminished glacier mass as a

consequence of global warming, as evidenced in Figure 2b, which shows a significant decrease in *IWSA* in the Tianshan Mountains [49,50]. Concurrently, a substantial volume of glacier meltwater contributes to surface runoff in the surrounding regions [51], thereby increasing the surface water area [52,53], which in turn leads to an increase of *SWSA* in the northern Tarim River Basin (Figure 2c). Meanwhile, the NDVI results indicate that the farmland area in the Tarim River Basin has been continuously expanding, mainly concentrated in the northern and western basins (see Figure 2d). As the SWS cannot satisfy the growing water demand, groundwater has become a significant source of agricultural irrigation [45,54].

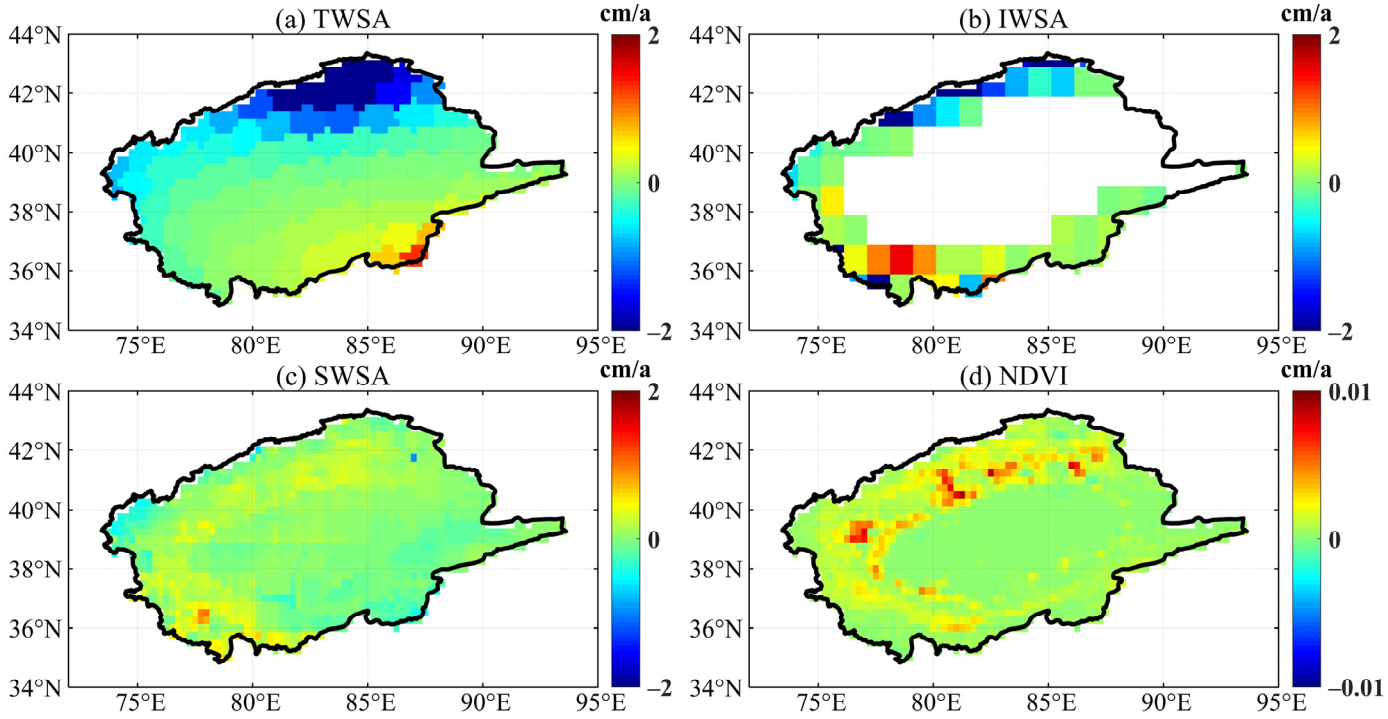

Figure 2. Spatial changes of water storage and NDVI in the Tarim River Basin. Among them, *IWSA* is only given for the period from April 2002 to January 2020, while the remaining data are all given for the period from April 2002 to December 2022.

The temporal changes of *SWSA*, *IWSA*, *GWSA-SI*, and *TWSA* in the Tarim River Basin are shown in Figure 3, and the statistical data are presented in Table 3. The contribution rate is calculated by dividing the trend of each water storage anomaly by the trend of *TWSA*, and their root mean square error (RMSE) and correlation coefficient (*CC*) are also counted in Table 3. This study divides the periods with January 2010 as the boundary. Figure 3 and Table 3 show that *TWSA* exhibited a severe declining trend at a rate of -0.48 ± 0.13 cm/a from April 2002 to December 2009. During this period, *SWSA* and *GWSA-SI* decreased at rates of -0.12 ± 0.04 cm/a and -0.42 ± 0.10 cm/a, respectively, contributing 25.0% and 87.5% to the decline of *TWSA*. Subsequently, from January 2010 to January 2020, the contribution of *IWSA* to *TWSA* increased by almost 70.0% compared to that from April 2002 to December 2009. Meanwhile, the rate of *GWSA-SI* decline recovered to -0.17 ± 0.07 cm/a and contributed 48.6% to the *TWSA*.

Additionally, this study found that the trend of *TWSA* reached -0.70 ± 0.31 cm/a during the period from 2020 to 2022, which tended to accelerate the loss of *TWSA* compared to the preceding two periods. The results indicate that *TWSA* in the Tarim River Basin has been declining for a long time, and the deficit rate of *TWSA* has accelerated in recent years. The decline of *TWSA* is closely related to the decrease of *GWSA-SI*, with a *CC* of more than 0.85 in Table 3. After 2010, the reduction of *TWSA* was mainly affected by the decline of *IWSA*, which led to a large amount of glacier meltwater flowing into the rivers.

According to the China River Sediment Bulletin, the mean annual runoff of the Kaidu River, Aksu River, Yarkant River, Yurungkax River, and the mainstream of the Tarim River increased by 32.0%, 18.6%, 7.2%, 25.9%, and 45.4%, respectively, from 2010−2022 compared to 2003−2009. This suggests that glacier ablation contributed to the increase of *SWSA*. Notably, from 2020 to 2022, the runoff of the above rivers increased by 52.2~132.1%, which provided a basis for the accelerated ablation of glaciers.

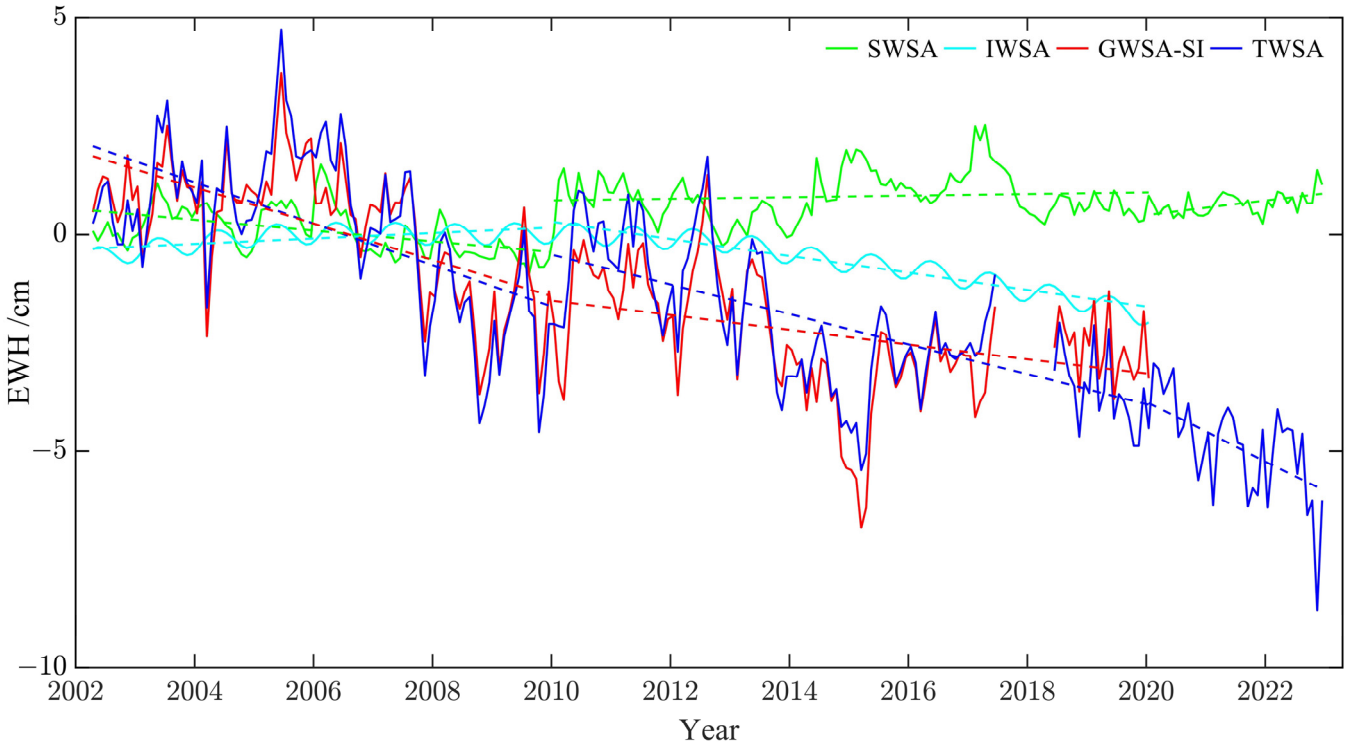

Figure 3. Temporal changes of water storage in the Tarim River Basin. The dotted lines are the trend lines for each water storage.

Table 3. Statistical results of the time series of water storage components.

Components	April 2002–December 2009			January 2010–January 2020			February 2020–December 2022
	Trend /cm·a^{-1}	Contribution Rate	*CC*	Trend /cm·a^{-1}	Contribution Rate	*CC*	Trend /cm·a^{-1}
TWSA	−0.48 ± 0.13	/	/	−0.35 ± 0.06	/	/	−0.70 ± 0.31
SWSA	−0.12 ± 0.04	25.0%	0.72	0.02 ± 0.03	−5.7%	−0.03	0.17 ± 0.09
IWSA	0.06 ± 0.01	−12.5%	0.12	−0.20 ± 0.01	57.1%	0.68	/
GWSA-SI	−0.42 ± 0.10	87.5%	0.96	−0.17 ± 0.07	48.6%	0.85	/

4.2. Comparative Analysis of Multi-Source GWSA

The depletion and recharge of *GWSA* in the Tarim River Basin is an important factor affecting *TWSA*, but there is uncertainty in the estimated *GWSA* based on GRACE/GFO. Therefore, this study introduces multiple measured *GWSA* (*GWSA-M*) for comparative analysis with the GRACE/GFO-derived *GWSA*. Figure 4 shows the temporal changes and trends of *GWSA*, *GWSA-SI*, and *GWSA-M*. In Figure 4a, *GWSA-M* declined at a rate of −0.23 ± 0.43 cm/a during the period from June 2018 to January 2020, and both *GWSA* and *GWSA-SI* also exhibited declining trends, with *GWSA-SI* decreasing approximately 31% slower than *GWSA*. For the long period from June 2018 to December 2021, the declining trend of *GWSA* reached −1.08 ± 0.34 cm/a, while the declining trend of *GWSA-M* reached

-0.34 ± 0.11 cm/a. This result suggests that the decline of *GWSA* would be overestimated were *IWSA* not accounted for in the analysis.

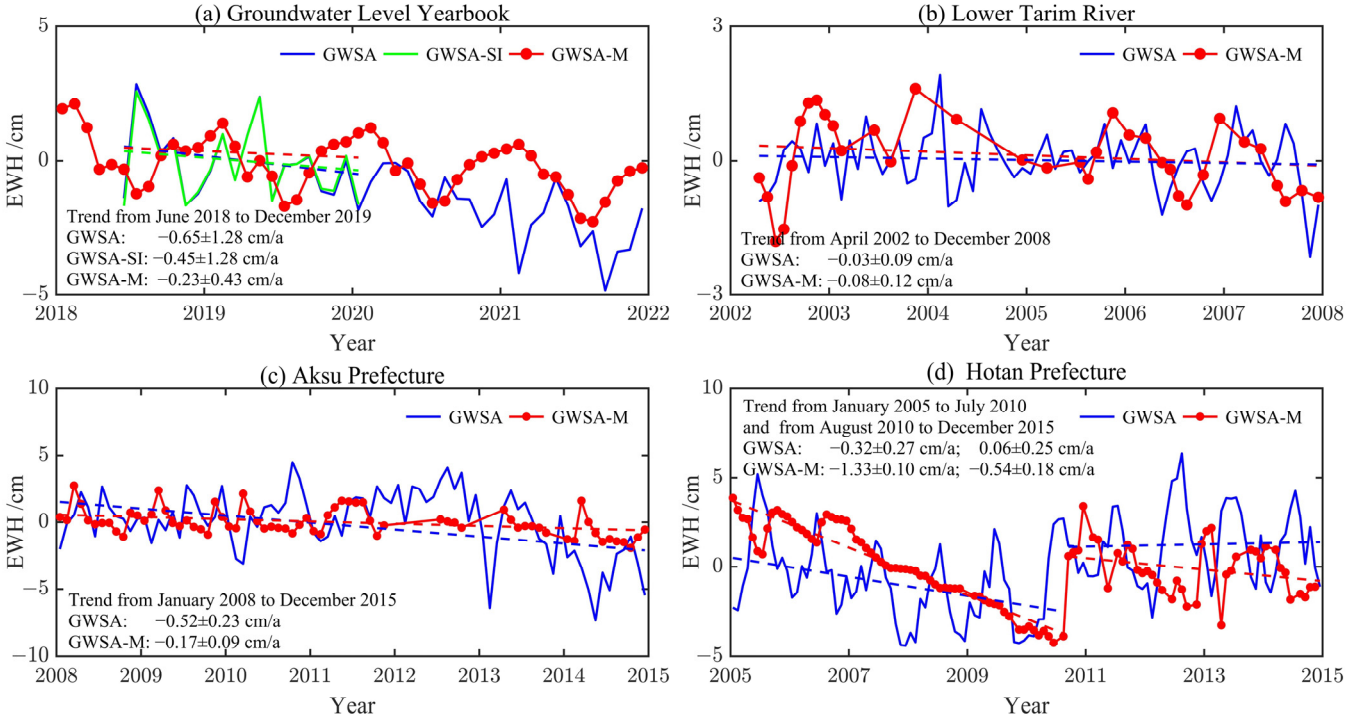

Figure 4. Temporal changes and trends of *GWSA*, *GWSA-SI*, and *GWSA-M*. The blue line is the *GWSA* derived from GRACE/GFO. The green line is the *GWSA* separated from *IWSA*. The red line is the *GWSA-M*. The dotted lines are the trend lines and their values have been recorded on each subplot figure.

Furthermore, we also introduce other measured groundwater data for comparative analysis. As shown in Figure 4b,c, *GWSA* and *GWSA-M* in the lower reaches of the Tarim River showed decreasing trends, and their RMSE reached 0.94 cm. *GWSA* and *GWSA-M* in the Aksu Prefecture continued to decline at rates of -0.52 ± 0.23 cm/a and -0.17 ± 0.09 cm/a, respectively. The lower levels of *GWSA* and *GWSA-M* in the Hotan Prefecture were concentrated in 2010. The above analysis reveals that the GRACE/GFO-derived *GWSA* is consistent with the *GWSA-M*.

5. Discussion

5.1. Independent Component Analysis of TWSA

To further confirm the main components affecting *TWSA* and the reasons for the accelerated depletion of *TWSA* in recent years, we employ the ICA method to decompose *TWSA* into independent components (ICs). The cumulative contribution rate of the first four ICs reaches 90.8%, which contains the primary information of *TWSA*. The spatiotemporal results of the ICs in Figure 5 demonstrate that IC1 exhibits an annual periodic signal primarily distributed in the Tianshan Mountains region. The *CC* between IC1 and *GWSA-SI* reaches its peak value of 0.70 between 2002 and 2009. After 2010, the *CC* between IC1 and *IWSA* is highest, at 0.69. This indicates that IC1 includes the signals of early groundwater depletion and late glacier mass loss in the Tianshan Mountains region. The IC2 signal is mainly concentrated in the Kunlun Mountains region, and its temporal components exhibit the highest *CC* with *IWSA* before and after 2010. This indicates that IC2 mainly contains the signals of glacier mass changes in the Kunlun Mountains region. The IC3 signal is located in the northern Tarim River Basin, and it is observed that the trend of IC3 is generally opposite to IC1. This suggests that IC3 represents the signal of glacier meltwater

replenishment in the Tianshan Mountains. While IC4 represents other signals with a long periodicity, it covers a large part of the basin, including the desert area.

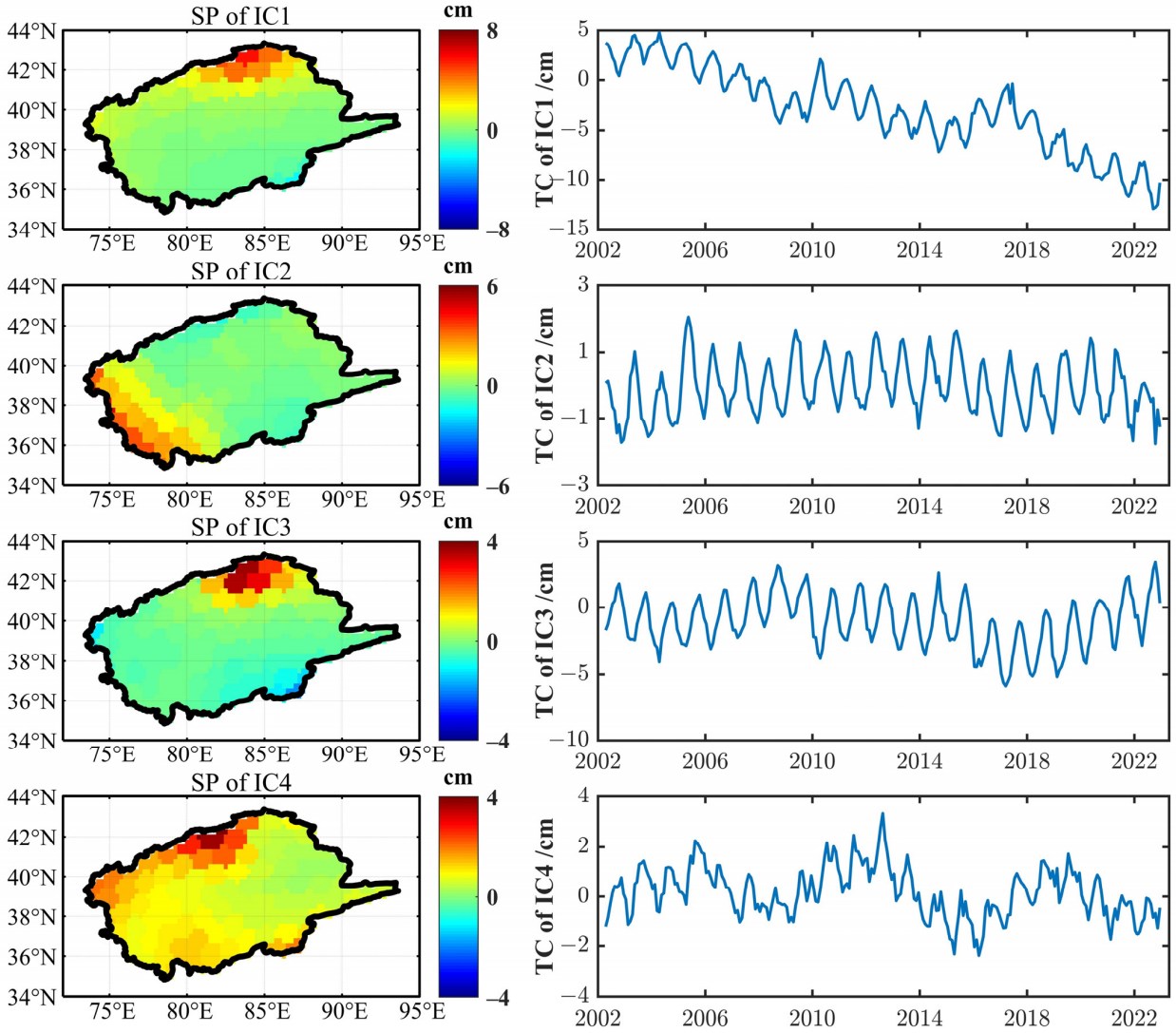

Figure 5. The spatial pattern (SP) and temporal component (TC) of the first four ICAs. The cumulative contribution rate of the first four ICs reaches 90.8%, among which the contribution rates of IC1 to IC4 reach 64.3%, 19.2%, 4.5%, and 2.8%, respectively.

The detailed ICA results confirm that the changes of groundwater storage and glacier mass are the main components of *TWSA* in the Tarim River Basin. Comparing the spatiotemporal components of IC1 and IC3, it is found that the difference in trends is more significant during the 2019−2022 period, and the contribution rate of the IC1 signal is much higher than that of IC3. Consequently, the accelerated melting of glaciers in the Tianshan Mountains region is a significant contributing factor to the accelerated depletion of *TWSA* in recent years.

5.2. Relationship Analysis Between Driving Factors and Water Storage Changes

The TWS changes in the Tarim River Basin are mainly attributed to the GWS and IWS changes, which are influenced by multiple driving factors. Therefore, the grey relation analysis (GRA) method investigates the correlation between various driving factors and *GWSC*/*IWSC* [55,56]. The associated factors include precipitation, evapotranspiration, NDVI, and water consumption. To unify the time scales of the datasets and eliminate their

unit effects, all data are converted to an annual scale and normalized by the max/min normalization approach.

As illustrated in Table 4, the results of the GRA indicate that the GRA coefficients between *GWSC* and annual precipitation are the most significant, with a maximum value of 0.74. Furthermore, the GRA coefficients between *GWSC* and human factors (NDVI and water consumption) are significantly higher than the GRA coefficients between *IWSC* and human factors. The factor most correlated with *IWSC* is annual evapotranspiration, and the GRA coefficients between *IWSC* and human factors are less than 0.60. These results indicate that *GWSC* is influenced by a combination of natural and human factors, while *IWSC* is mainly associated with natural factors.

Table 4. Grey relation analysis between natural/human factors and *GWSC*/*IWSC*.

Factors	*GWSC*		*IWSC*	
	GRA Coefficients	**Rank**	**GRA Coefficients**	**Rank**
Annual precipitation	0.74	1	0.65	2
Annual evapotranspiration	0.66	2	0.68	1
NDVI	0.63	4	0.55	3
Annual water consumption	0.64	3	0.53	4

To further investigate the impact of various driving factors on *GWSC* and *IWSC*, this study collected the annual changes in the above data (Figure 6). Figure 6a illustrates that *GWSC* exhibited notable declines during 2006−2009 and 2013−2014, and *IWSC* exhibited a consistent decline from 2003 to 2019. Regarding natural factors, Figure 6b shows that precipitation from 2006 to 2009 decreased by 7~21% compared to the entire period, and precipitation from 2013 to 2014 also decreased by 7~12% compared to the whole period. Additionally, evapotranspiration increased at a rate of 0.02 ± 0.07 mm/a from 2003 to 2019. These changes have resulted in a decrease in natural water inflows.

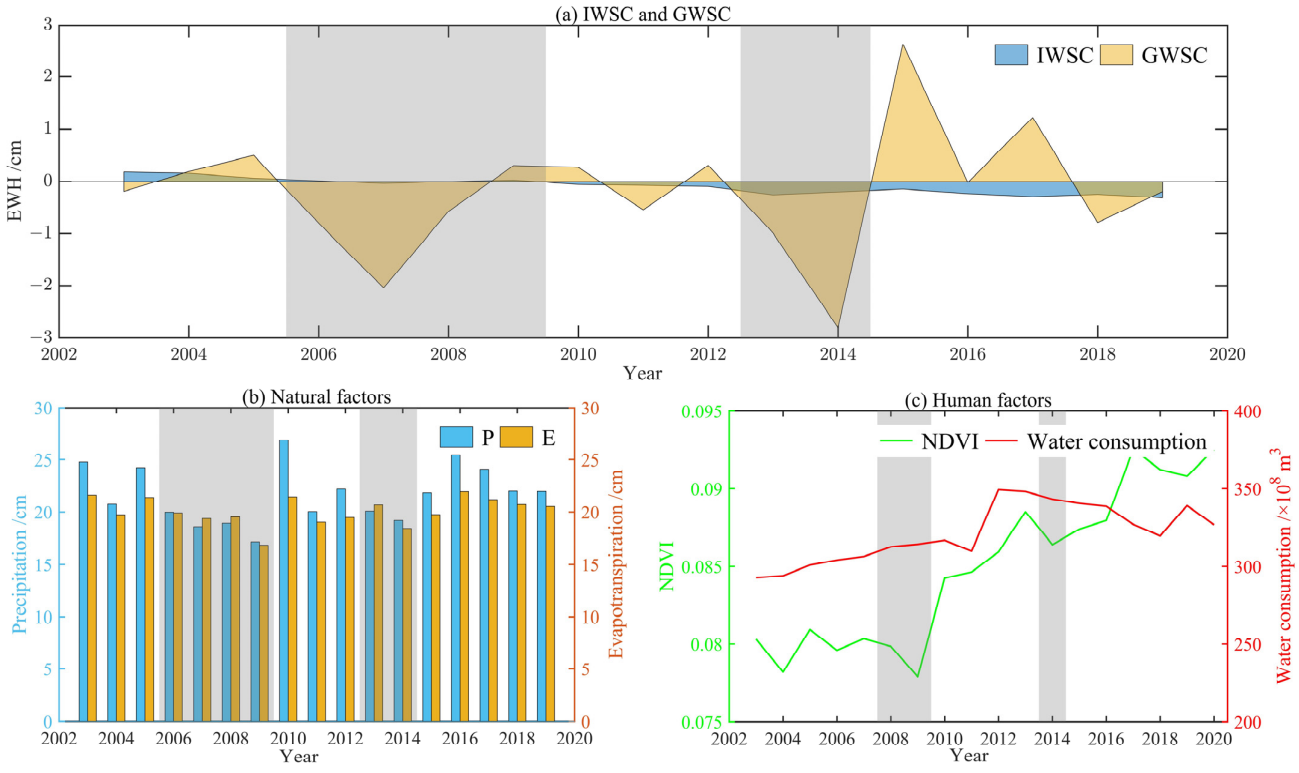

Figure 6. Annual changes of IWS, GWS, and natural/human factors in the Tarim River Basin. The shaded areas represent periods of notable declines in *GWSC*.

In terms of anthropogenic influences, the period from 2003 to 2019 witnessed a 13.1% increase in the NDVI and a 15.8% increase in water consumption. Notably, the periods of notable declines in *GWSC* (shaded in Figure 6c) coincided with rapid growth in water consumption, while NDVI reached a local peak. In contrast, *GWSA* showed two significant increases after 2014, where the first increase was influenced by the increase of glacier meltwater and precipitation, while the second increase was related to the glacier meltwater increase and human water consumption further decreased. Concerning long-term changes of human factors, their impacts on *GWSC* in the basin are gradually increasing. Therefore, it can be argued that *GWSC* is easily subject to significant depletion due to short-term effects, such as unexpected decreases in precipitation and rapid increases in human water consumption. In addition, the decline of *IWSC* is associated with the long-term increase of evapotranspiration, which tends to accelerate glacial melt.

5.3. Revealing the Feasibility of EWC Benefits Through GRACE/GFO Data

Statistically, the EWC project has been implemented 23 times from 2000 to 2022 and cumulatively conveyed about 9.5 billion m^3 of ecological water to the lower reaches of the Tarim River, resulting in the migration of TWS. This volume of EWC is considerable for the small area of the lower reaches of the Tarim River, which provides the possibility for GRACE/GFO detection. Therefore, this study applies GRACE/GFO data in the lower reaches of the Tarim River to assess the viability of monitoring EWC benefits. Due to the spatial resolution limitations of GRACE/GFO and the specific location of the ecological water source, we designate the study area within the red frame in Figure 1 as the lower reaches of the Tarim River, with a grid size of $1.8^\circ \times 1.3^\circ$.

Figure 7 shows the temporal changes of *TWSA*, GRACE-DSI, NDVI, and EWC in the lower reaches of the Tarim River, where the EWC represents the monthly average value of each EWC. According to the volume of EWC, the interval from 2007 to 2015 is regarded as the lower EWC period, while the remaining period is regarded as the normal EWC period. During the lower EWC period, *TWSA* exhibited a declining trend, intensifying the aridity of the lower reaches of Tarim River. In particular, the significant decline of EWC from 2007 to 2009 resulted in a *TWSA* decline rate of -0.62 ± 0.19 cm/a. This led to the basin experiencing the most severe drought in the last 20 years by the end of 2009. Meanwhile, the areas of surface water, seasonal water, and permanent water all reached local minima in 2009 [57]. In contrast, during the normal EWC period, the increased frequency of EWC and the changes of the EWC approach led to a significant increase in EWC volume. Compared to the lower EWC period, the average EWC and NDVI trend in the normal EWC period increased by 59.0% and 60.0%, respectively.

In addition, Figure 7a marks the temporal node of exceptional drought, extreme drought, and severe drought events corresponding to the drought index. Evidently, these drought events mainly occurred during 2009−2010 and 2014−2015, coinciding with significant deficits of EWC. Meanwhile, according to the drought frequency statistics in Figure 7c, the drought severity during the normal EWC period had improved significantly compared to the lower EWC period. The frequencies of exceptional drought, extreme drought, severe drought, moderate drought, and abnormally dry conditions decreased by 2.0%, 5.7%, 3.1%, 11.1%, and 8.7% respectively, indicating a 30.6% reduction in the total frequency of drought conditions in the lower reaches of the Tarim River.

From a water balance perspective, this study formulates the water balance equation for the lower reaches of the Tarim River based on precipitation (P), evapotranspiration (E), and EWC. The annual *TWSC*, net precipitation (P − E), water balance result (P − E + EWC), and runoff are shown in Figure 8. It is observed that evapotranspiration consistently exceeds precipitation in the lower reaches of the Tarim River, while the implementation of EWC could effectively alleviate the local water shortage. Comparative analysis reveals that compared to net precipitation, the water balance result is 36.6% lower in RMSE with *TWSC* and 24.8% higher in *CC* with *TWSC*, which reveals that *TWSC* contains the impacts of EWC. Combined with the measured runoff of the Tarim River mainstream

(Figure 8), it becomes evident that the temporal changes of the runoff and water balance result have a strong consistency, with a *CC* of 0.66, and the *CC* between the runoff and EWC reaches 0.68. This suggests that the EWC change is closely associated with the runoff of the Tarim River mainstream.

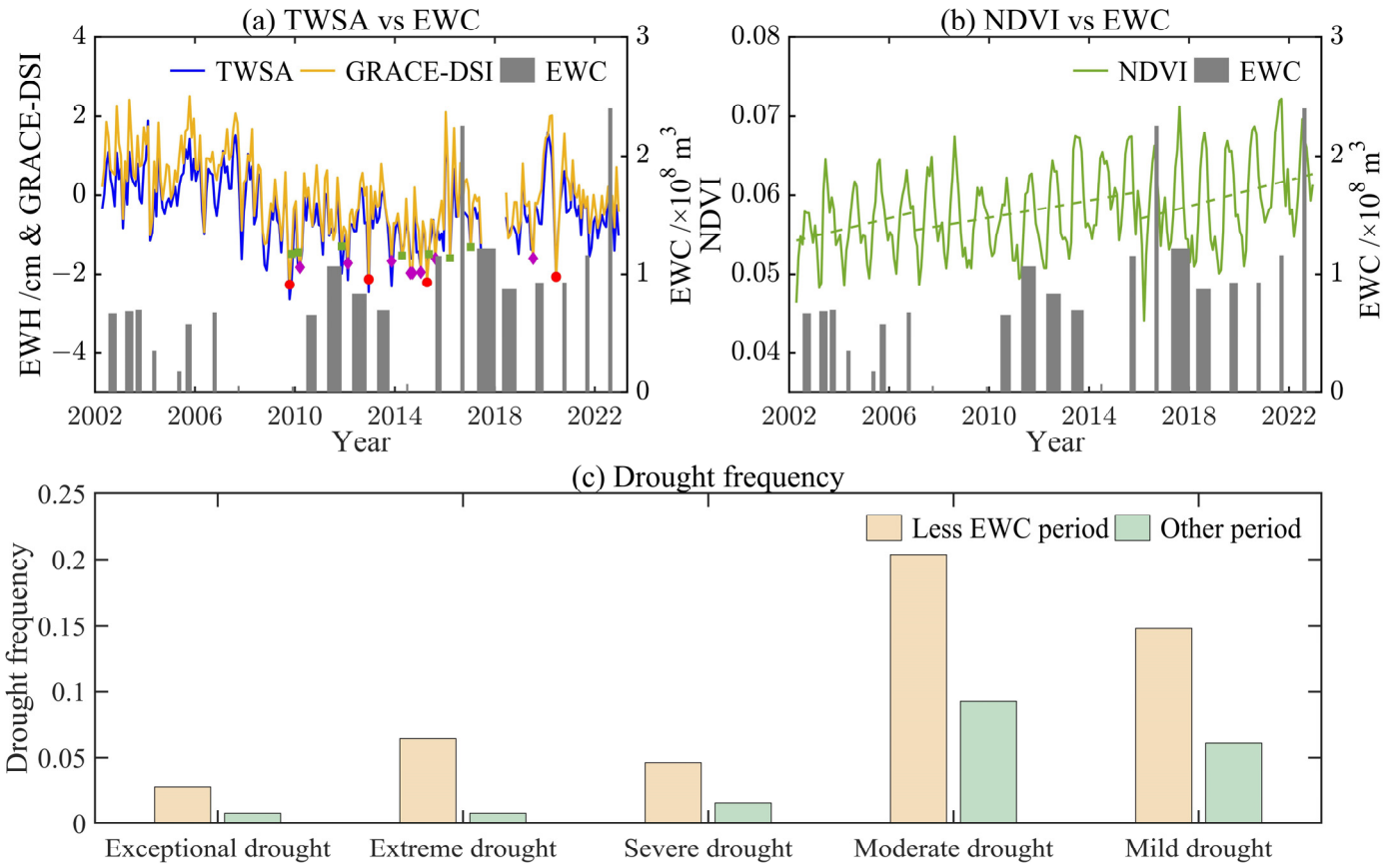

Figure 7. Temporal changes of *TWSA*, NDVI, and EWC, and the frequency of drought conditions in the lower reaches of the Tarim River. (**a**) The red dots represent exceptional drought, the purple diamonds represent extreme drought, and the green squares represent severe drought. (**b**) Temporal changes of NDVI and EWC, and the green dotted lines indicate the trends of NDVI during the periods. (**c**) The frequency of drought conditions in the lower reaches of the Tarim River.

Figure 9a shows the temporal changes of GRACE/GFO-derived *GWSA* and EWC. During the lower EWC period, the annual mean *GWSA* reduced by 0.91 cm compared to 2003−2006. Subsequently, the annual mean *GWSA* shows a reduction, reaching a value of 0.35 cm between 2016 and 2022. In particular, two local minima in *GWSA* were observed in the 2009−2010 and 2014−2015 periods. These phenomena can be attributed to the extremely low EWC in 2009 and 2014, coupled with the lagged response of *GWSA* to reflect the implementation of EWC in the latter halves of 2010 and 2015 [58,59].

To ensure the reliability of the GRACE/GFO data, this study also introduces measured groundwater data from the lower reaches of the Tarim River for comparison analysis. In particular, Figure 9b illustrates the annual changes of measured groundwater depth within the Yingsu and Alagan regions [60]. The findings revealed that both *GWSA* and measured groundwater data exhibited local minima in 2009−2010 and 2014−2015, which also coincides with the results of the literature [59] on measured groundwater data in the lower reaches of the Tarim River. Regarding long-term changes, the measured groundwater data show an increasing trend after 2010, and the GRACE/GFO-derived *GWSA* trend also increased by 0.20 cm/a after 2010 compared to the pre-2010 period. Therefore, the GRACE/GFO-derived *TWSA* in the lower reaches of the Tarim River has a good corre-

spondence with the changes of EWC, NDVI, and measured groundwater, which indicates GRACE/GFO can effectively detect the impacts of EWC.

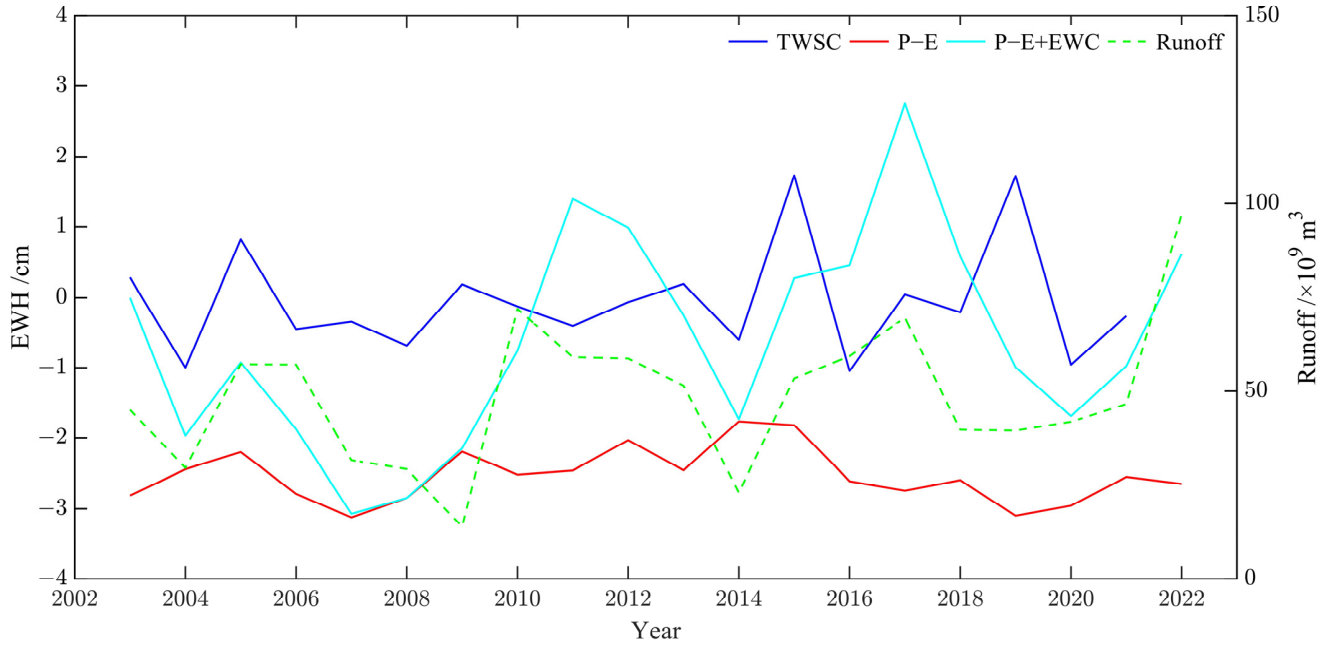

Figure 8. Annual *TWSC*, net precipitation (P − E), water balance result (P − E + EWC), and runoff of the Tarim River mainstream.

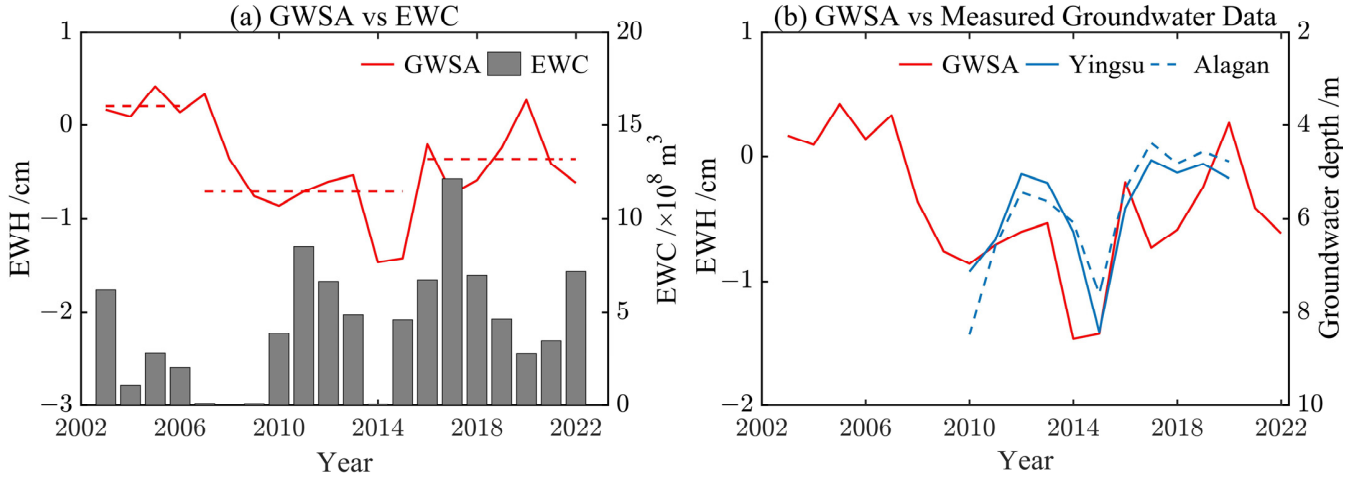

Figure 9. Annual changes of *GWSA* and EWC. (**a**) The red line is the annual averages of GRACE/GFO-derived *GWSA*, red dotted lines indicate the annual mean of *GWSA* during the periods. (**b**) The blue lines indicate the measured groundwater depth.

6. Conclusions

This study analyzes the spatiotemporal changes of water storage and its driving factors in the Tarim River Basin based on multi-source hydrological data. In addition, we explore the feasibility of evaluating the regional EWC benefit based on GRACE/GFO satellite gravity observations, which provides a reference for subsequent research to evaluate EWH benefit. The main conclusions are as follows.

(1) Spatial analysis reveals a significant depletion of *TWSA* and *IWSA* in the northern Tarim River Basin, while *SWSA* was stable overall and NDVI continued to increase. Temporal analysis indicates that the basin has exhibited a long-term *TWSA* deficit, which appears to have accelerated in recent years. Among the water storage compo-

nents, *GWSA* contributes over 50% to *TWSA* on average, and the contribution of *IWSA* to *TWSA* has increased significantly since 2010. In addition, the ICA results suggest that the changes of groundwater storage and glacier mass are the main components of *TWSA* in the basin and show that the accelerated glacier melting in the Tianshan Mountains identified as a key driver of *TWSA* depletion in recent years.

(2) The TWS change in the Tarim River Basin is primarily attributed to the changes of GWS and IWS. The driving factor analysis reveals that *GWSC* and *IWSC* exhibit the strongest correlations with precipitation and evapotranspiration, with grey relation analysis (GRA) coefficients of 0.74 and 0.68, respectively. Human factors, including the NDVI and water consumption, mainly affect *GWSC*, with an average GRA coefficient of 0.64. It is plausible to suggest that *GWSC* is particularly susceptible to substantial depletion due to short-term fluctuations, such as abrupt reductions in precipitation and rapid increases in human water consumption. In addition, the decline of *IWSC* is associated with the long-term increase of evapotranspiration.

(3) During the lower EWC period from 2007 to 2015, GRACE/GFO-derived *TWSA* showed a marked decline in the lower reaches of the Tarim River. In contrast, during the normal EWC periods from 2002 to 2006 and 2016 to 2022, there was a significant increase in both EWC and the NDVI, resulting in a 30.6% reduction in drought frequency. Additionally, the integration of EWC data led to a 36.6% reduction in the RMSE between the water balance result and *TWSC* and a 24.8% enhancement in their *CC*. Furthermore, GRACE/GFO-derived *GWSA* shows a good correspondence with the measured groundwater data. Therefore, we demonstrate the feasibility of using GRACE/GFO to effectively reveal the benefits of EWC in the lower reaches of the Tarim River.

Author Contributions: Both authors collaborated to conduct this study. W.S.: data collection, scientific analysis, manuscript writing, and editing. X.Z.: experiment design, methodology, review, and editing. All authors have read and agreed to the published version of the manuscript.

Funding: This research was funded by the National Natural Science Foundation of China, grant number 42074003 and 42374100.

Data Availability Statement: Data sources are contained in Table 1 in the article.

Acknowledgments: The authors would like to sincerely thank the developers of GRACE, GLDAS, and glacier water models, and also thank the researchers who provided the ERA5 reanalysis dataset and measured groundwater dataset.

Conflicts of Interest: The authors declare no conflicts of interest.

References

1. Rodell, M.; Reager, J.T. Water cycle science enabled by the GRACE and GRACE-FO satellite missions. *Nat. Water* **2023**, *1*, 47–59. [CrossRef]
2. Chandanpurkar, H.A.; Reager, J.T.; Famiglietti, J.S.; Nerem, R.S.; Chambers, D.P.; Lo, M.-H.; Hamlington, B.D.; Syed, T.H. The Seasonality of Global Land and Ocean Mass and the Changing Water Cycle. *Geophys. Res. Lett.* **2021**, *48*, e2020GL091248. [CrossRef]
3. Humphrey, V.; Gudmundsson, L.; Seneviratne, S.I. Assessing Global Water Storage Variability from GRACE: Trends, Seasonal Cycle, Subseasonal Anomalies and Extremes. *Surv. Geophys.* **2016**, *37*, 357–395. [CrossRef]
4. Chen, Z.; Jiang, W.; Wu, J.; Chen, K.; Deng, Y.; Jia, K.; Mo, X. Detection of the spatial patterns of water storage variation over China in recent 70 years. *Sci. Rep.* **2017**, *7*, 6423. [CrossRef] [PubMed]
5. Wang, J.; Chen, Y. The applicability of using NARX neural network to forecast GRACE terrestrial water storage anomalies. *Nat. Hazards* **2022**, *110*, 1997–2016. [CrossRef]
6. Ahmed, M.; Sultan, M.; Elbayoumi, T.; Tissot, P. Forecasting GRACE Data over the African Watersheds Using Artificial Neural Networks. *Remote Sens.* **2019**, *11*, 1769. [CrossRef]
7. Hosseini-Moghari, S.-M.; Araghinejad, S.; Ebrahimi, K.; Tang, Q.; AghaKouchak, A. Using GRACE satellite observations for separating meteorological variability from anthropogenic impacts on water availability. *Sci. Rep.* **2020**, *10*, 15098. [CrossRef]
8. Wang-Erlandsson, L.; Tobian, A.; van der Ent, R.J.; Fetzer, I.; te Wierik, S.; Porkka, M.; Staal, A.; Jaramillo, F.; Dahlmann, H.; Singh, C.; et al. A planetary boundary for green water. *Nat. Rev. Earth Environ.* **2022**, *3*, 380–392. [CrossRef]

9. Sun, S.; Wang, Y.; Liu, J.; Cai, H.; Wu, P.; Geng, Q.; Xu, L. Sustainability assessment of regional water resources under the DPSIR framework. *J. Hydrol.* **2016**, *532*, 140–148. [CrossRef]
10. Bai, Y.; Wang, Y.; Chen, Y.; Zhang, L. Probabilistic analysis of the controls on groundwater depth using Copula Functions. *Hydrol. Res.* **2020**, *51*, 406–422. [CrossRef]
11. Chen, Y.; Ye, Z.; Shen, Y. Desiccation of the Tarim River, Xinjiang, China, and mitigation strategy. *Quat. Int.* **2011**, *244*, 264–271. [CrossRef]
12. Ye, Z.X.; Chen, Y.N.; Li, W.H.; Yan, Y.; Wan, J.H. Groundwater fluctuations induced by ecological water conveyance in the lower Tarim River, Xinjiang, China. *J. Arid. Environ.* **2009**, *73*, 726–732. [CrossRef]
13. Wang, Q.; Yi, S.; Sun, W. Continuous Estimates of Glacier Mass Balance in High Mountain Asia Based on ICESat-1,2 and GRACE/GRACE Follow-On Data. *Geophys. Res. Lett.* **2021**, *48*, e2020GL090954. [CrossRef]
14. Jakob, L.; Gourmelen, N.; Ewart, M.; Plummer, S. Spatially and temporally resolved ice loss in High Mountain Asia and the Gulf of Alaska observed by CryoSat-2 swath altimetry between 2010 and 2019. *Cryosphere* **2021**, *15*, 1845–1862. [CrossRef]
15. Ren, P.; Pan, X.; Liu, T.; Huang, Y.; Chen, X.; Wang, X.; Chen, P.; Akmalov, S. Glacier Changes from 1990 to 2022 in the Aksu River Basin, Western Tien Shan. *Remote Sens.* **2024**, *16*, 1751. [CrossRef]
16. Chen, Z.; Zhang, X.; Chen, J. Monitoring Terrestrial Water Storage Changes with the Tongji-Grace 2018 Model in the Nine Major River Basins of the Chinese Mainland. *Remote Sens.* **2021**, *13*, 1851.
17. Williams, S.D.P.; Moore, P.; King, M.A.; Whitehouse, P.L. Revisiting GRACE Antarctic ice mass trends and accelerations considering autocorrelation. *Earth Planet. Sci. Lett.* **2014**, *385*, 12–21. [CrossRef]
18. Jeon, T.; Seo, K.-W.; Youm, K.; Chen, J.; Wilson, C.R. Global sea level change signatures observed by GRACE satellite gravimetry. *Sci. Rep.* **2018**, *8*, 13519. [CrossRef]
19. Yang, T.; Wang, C.; Chen, Y.; Chen, X.; Yu, Z. Climate change and water storage variability over an arid endorheic region. *J. Hydrol.* **2015**, *529*, 330–339. [CrossRef]
20. Zuo, J.; Xu, J.; Chen, Y.; Li, W. Downscaling simulation of groundwater storage in the Tarim River basin in northwest China based on GRACE data. *Phys. Chem. Earth Parts A/B/C* **2021**, *123*, 103042. [CrossRef]
21. Xu, M.; Wang, X.; Sun, T.; Wu, H.; Li, X.; Kang, S. Water balance change and its implications to vegetation in the Tarim River Basin, Central Asia. *Quat. Int.* **2019**, *523*, 25–36. [CrossRef]
22. Yang, P.; Xia, J.; Zhan, C.; Qiao, Y.; Wang, Y. Monitoring the spatio-temporal changes of terrestrial water storage using GRACE data in the Tarim River basin between 2002 and 2015. *Sci. Total Environ.* **2017**, *595*, 218–228. [CrossRef] [PubMed]
23. Chen, Z.; Zheng, W.; Yin, W.; Li, X.; Ma, M. Improving Spatial Resolution of GRACE-Derived Water Storage Changes Based on Geographically Weighted Regression Downscaled Model. *IEEE J. Sel. Top. Appl. Earth Obs. Remote Sens.* **2023**, *16*, 4261–4275. [CrossRef]
24. Xue, L.; Yang, F.; Yang, C.; Chen, X.; Zhang, L.; Chi, Y.; Yang, G. Identification of potential impacts of climate change and anthropogenic activities on streamflow alterations in the Tarim River Basin, China. *Sci. Rep.* **2017**, *7*, 8254. [CrossRef]
25. Wang, F.; Chen, Y.; Li, Z.; Fang, G.; Peng, L.; Wang, X.; Zhang, X.; Kayumba Patient, M. Developing a Long Short-Term Memory (LSTM)-Based Model for Reconstructing Terrestrial Water Storage Variations from 1982 to 2016 in the Tarim River Basin, Northwest China. *Remote Sens.* **2021**, *13*, 889. [CrossRef]
26. Yao, J.; Hu, W.; Chen, Y.; Huo, W.; Zhao, Y.; Mao, W.; Yang, Q. Hydro-climatic changes and their impacts on vegetation in Xinjiang, Central Asia. *Sci. Total Environ.* **2019**, *660*, 724–732. [CrossRef]
27. Zhao, K.; Li, X. Estimating terrestrial water storage changes in the Tarim River Basin using GRACE data. *Geophys. J. Int.* **2017**, *211*, 1449–1460. [CrossRef]
28. Cheng, W.; Feng, Q.; Xi, H.; Yin, X.; Sindikubwabo, C.; Habiyakare, T.; Chen, Y.; Zhao, X. Spatiotemporal variability and controlling factors of groundwater depletion in endorheic basins of Northwest China. *J. Environ. Manag.* **2023**, *344*, 118468. [CrossRef]
29. Wan, L.; Bento, V.A.; Qu, Y.; Qiu, J.; Song, H.; Zhang, R.; Wu, X.; Xu, F.; Lu, J.; Wang, Q. Drought characteristics and dominant factors across China: Insights from high-resolution daily SPEI dataset between 1979 and 2018. *Sci. Total Environ.* **2023**, *901*, 166362. [CrossRef]
30. Fallah, B.; Russo, E.; Menz, C.; Hoffmann, P.; Didovets, I.; Hattermann, F.F. Anthropogenic influence on extreme temperature and precipitation in Central Asia. *Sci. Rep.* **2023**, *13*, 6854. [CrossRef]
31. Zhuang, L.; Ke, C.; Cai, Y.; Nourani, V. Measuring glacier changes in the Tianshan Mountains over the past 20 years using Google Earth Engine and machine learning. *J. Geogr. Sci.* **2023**, *33*, 1939–1964. [CrossRef]
32. Xu, H.; Ye, M.; Li, J. Changes in groundwater levels and the response of natural vegetation to transfer of water to the lower reaches of the Tarim River. *J. Environ. Sci.* **2007**, *19*, 1199–1207. [CrossRef] [PubMed]
33. Chen, Y.; Wumaierjiang, W.; Aikeremu, A.; Cheng, Y.; Chen, Y.; Hao, X.; Zhu, C.; Wang, Y. Monitoring and analysis of ecological benefits of water conveyance in the lower reaches of Tarim River in recent 20 years. *Arid. Land Geogr.* **2021**, *44*, 605–611. [CrossRef]
34. Guo, H.; Jiapaer, G.; Bao, A.; Li, X.; Huang, Y.; Ndayisaba, F.; Meng, F. Effects of the Tarim River's middle stream water transport dike on the fractional cover of desert riparian vegetation. *Ecol. Eng.* **2017**, *99*, 333–342. [CrossRef]
35. Zhang, X.; Zuo, Q. Analysis of Water Resource Situation of the Tarim River Basin and the System Evolution under the Changing Environment. *J. Coast. Res.* **2015**, *73*, 9–16. [CrossRef]

36. Li, W.; Huang, F.; Shi, F.; Wei, X.; Zamanian, K.; Zhao, X. Human and climatic drivers of land and water use from 1997 to 2019 in Tarim River basin, China. *Int. Soil Water Conserv. Res.* **2021**, *9*, 532–543. [CrossRef]
37. Feng, Q.; Liu, W.; Si, J.; Su, Y.; Zhang, Y.; Cang, Z.; Xi, H. Environmental effects of water resource development and use in the Tarim River basin of northwestern China. *Environ. Geol.* **2005**, *48*, 202–210. [CrossRef]
38. Chen, Y.; Hao, X.; Chen, Y.; Zhu, C. Study on Water System Connectivity and Ecological Protection Countermeasures of Tarim River Basin in Xinjiang. *Bull. Chin. Acad. Sci.* **2019**, *34*, 1156–1164. [CrossRef]
39. Save, H.; Bettadpur, S.; Tapley, B.D. High-resolution CSR GRACE RL05 mascons. *J. Geophys. Res. Solid Earth* **2016**, *121*, 7547–7569. [CrossRef]
40. Hugonnet, R.; McNabb, R.; Berthier, E.; Menounos, B.; Nuth, C.; Girod, L.; Farinotti, D.; Huss, M.; Dussaillant, I.; Brun, F.; et al. Accelerated global glacier mass loss in the early twenty-first century. *Nature* **2021**, *592*, 726–731. [CrossRef]
41. Chen, Y.; Hao, X. *Dataset of Groundwater Level in the Lower Reaches of Tarim River (2000–2007)*; National Tibetan Plateau/Third Pole Environment Data Center: Beijing, China, 2021. [CrossRef]
42. Zhu, Z.; Tang, X.; Yuan, G.; Zhang, X.; Sun, X. *Chinese Ecosystem Research Network 2005–2014 Groundwater Data Set*; Science Data Bank: Beijing, China, 2016. [CrossRef]
43. Yi, S.; Sneeuw, N. Filling the Data Gaps Within GRACE Missions Using Singular Spectrum Analysis. *J. Geophys. Res. Solid Earth* **2021**, *126*, e2020JB021227. [CrossRef]
44. Su, Y.; Guo, B.; Zhou, Z.; Zhong, Y.; Min, L. Spatio-Temporal Variations in Groundwater Revealed by GRACE and Its Driving Factors in the Huang-Huai-Hai Plain, China. *Sensors* **2020**, *20*, 922. [CrossRef] [PubMed]
45. Li, Q.; Pan, Y.; Zhang, C.; Gong, H. Quantifying Multi-Source Uncertainties in GRACE-Based Estimates of Groundwater Storage Changes in Mainland China. *Remote Sens.* **2023**, *15*, 2744. [CrossRef]
46. Feng, T.; Shen, Y.; Chen, Q.; Wang, F.; Zhang, X. Groundwater storage change and driving factor analysis in north china using independent component decomposition. *J. Hydrol.* **2022**, *609*, 127708. [CrossRef]
47. Forootan, E.; Kusche, J.; Loth, I.; Schuh, W.-D.; Eicker, A.; Awange, J.; Longuevergne, L.; Diekkrüger, B.; Schmidt, M.; Shum, C.K. Multivariate Prediction of Total Water Storage Changes Over West Africa from Multi-Satellite Data. *Surv. Geophys.* **2014**, *35*, 913–940. [CrossRef]
48. Zhao, M.; Geruo, A.; Velicogna, I.; Kimball, J.S. Satellite Observations of Regional Drought Severity in the Continental United States Using GRACE-Based Terrestrial Water Storage Changes. *J. Clim.* **2017**, *30*, 6297–6308. [CrossRef]
49. Xiang, L.; Wang, H.; Steffen, H.; Jiang, L.; Shen, Q.; Jia, L.; Su, Z.; Wang, W.; Deng, F.; Qiao, B.; et al. Two Decades of Terrestrial Water Storage Changes in the Tibetan Plateau and Its Surroundings Revealed through GRACE/GRACE-FO. *Remote Sens.* **2023**, *15*, 3505. [CrossRef]
50. Liu, Q.; Xu, Y.; Chen, J.; Cheng, X. Multi-source satellite reveals the heterogeneity in water storage change over northwestern China in recent decades. *J. Hydrol.* **2023**, *624*, 129953. [CrossRef]
51. Wang, X.; Luo, Y.; Sun, L.; Shafeeque, M. Different climate factors contributing for runoff increases in the high glacierized tributaries of Tarim River Basin, China. *J. Hydrol. Reg. Stud.* **2021**, *36*, 100845. [CrossRef]
52. Luo, Y.; Wang, X.; Piao, S.; Sun, L.; Ciais, P.; Zhang, Y.; Ma, C.; Gan, R.; He, C. Contrasting streamflow regimes induced by melting glaciers across the Tien Shan—Pamir—North Karakoram. *Sci Rep.* **2018**, *8*, 16470. [CrossRef]
53. Lu, S.; Wang, Y.; Zhou, J.; Hughes, A.C.; Li, M.; Du, C.; Yang, X.; Xiong, Y.; Zi, F.; Wang, W.; et al. Active water management brings possibility restoration to degraded lakes in dryland regions: A case study of Lop Nur, China. *Sci. Rep.* **2022**, *12*, 18578. [CrossRef] [PubMed]
54. Wang, W.; Chen, Y.; Wang, W. Groundwater recharge in the oasis-desert areas of northern Tarim Basin, Northwest China. *Hydrol. Res.* **2020**, *51*, 1506–1520. [CrossRef]
55. Chen, X.; Jiang, J.; Lei, T.; Yue, C. GRACE satellite monitoring and driving factors analysis of groundwater storage under high-intensity coal mining conditions: A case study of Ordos, northern Shaanxi and Shanxi, China. *Hydrogeol. J.* **2020**, *28*, 673–686. [CrossRef]
56. Liu, R.; Zhong, B.; Li, X.; Zheng, K.; Liang, H.; Cao, J.; Yan, X.; Lyu, H. Analysis of groundwater changes (2003–2020) in the North China Plain using geodetic measurements. *J. Hydrol. Reg. Stud.* **2022**, *41*, 101085. [CrossRef]
57. Zou, S.; Abuduwaili, J.; Huang, W.; Duan, W. Effects of ecological water conveyance on changes of surface water area in the lower reaches of Tarim River. *Arid. Land Geogr.* **2021**, *44*, 681–690. [CrossRef]
58. Zhu, C.; Shen, Q.; Zhang, K.; Zhang, X.; Li, J. Multiscale Detection and Assessment of Vegetation Eco-Environmental Restoration following Ecological Water Compensation in the Lower Reaches of the Tarim River, China. *Remote Sens.* **2022**, *14*, 5855. [CrossRef]
59. Chen, Y.; Chen, Y.; Zhu, C.; Wang, Y.; Hao, X. Ecohydrological effects of water conveyance in a disconnected river in an arid inland river basin. *Sci. Rep.* **2022**, *12*, 9982. [CrossRef]
60. Di, Z.; Xie, Z.; Chen, Y. Estimation of riparian groundwater table depth in the lower reaches of Tarim River under long-term water conveyance. *Arid. Land Geogr.* **2021**, *44*, 659–669.